Article:
Avan, E.Y., Spencer, A., Dwyer-Joyce, R.S. et al. (2 more authors) (2013) Experimental and numerical investigations of oil film formation and friction in a piston ring-liner contact. Proceedings of the Institution of Mechanical Engineers, Part J: Journal of Engineering Tribology, 227 (2). pp. 126-140. ISSN 1350-6501

https://doi.org/10.1177/1350650112464706

Experimental and Numerical Investigations of a Simulated Piston Ring-Liner Contact

Emin Yusuf Avan[1*], Andrew Spencer[2*], Rob S Dwyer-Joyce[1], Andreas Almqvist[2], and Roland Larsson[2]

[1]The Leonardo Centre for Tribology, Department of Mechanical Engineering, University of Sheffield, Sheffield, UK
[2]Division of Machine Elements, Luleå University of Technology, Luleå, Sweden
[*]Corresponding authors, email: e.y.avan@shef.ac.uk, andrew.spencer@ltu.se

Abstract

The piston ring-cylinder liner contact is a major source of the total parasitic losses in an internal combustion engine. The lubrication regime formed in this contact is critical to the amount of friction, oil consumption and wear that occurs. In this work, a reciprocating test rig combined with an ultrasonic film thickness measurement system was used for the tribological investigation of the piston ring-cylinder liner contact. Furthermore, a numerical model has been developed for all lubrication regimes to predict the film thickness and friction. A special piston ring and cylinder liner holder were designed and five sensors were glued on to the back side of the liner specimen. Ultrasonic reflections captured by the sensors, used to obtain the film thickness and friction were continuously recorded as the piston ring reciprocated over the liner. Several experiments have been performed at different speed and load conditions. The experimentally measured film thickness and friction are compared with the output from the numerical model and good correlation is found. The parameters affecting the accurate measurement and simulation of film thickness and friction are then discussed.

1 Introduction

The piston ring-cylinder liner conjunction in an internal combustion engine is very important for the automotive industry in the drive to increase engine efficiency and achieve the emission reduction targets proposed by authorities. Piston rings operate in a range of tribological conditions, from the boundary to hydrodynamic lubrication regime. The operating temperature reaches about 200°C or more, and the piston speed varies from zero to up to approximately 20 m/s, depending on engine type. At these conditions, the piston rings should provide a mechanical seal between the combustion chamber and engine crankcase, conduct the heat of the piston to the water-cooled cylinder liner, and also distribute the lubricating oil along the cylinder liner. The optimum lubrication of the piston

rings is necessary to reduce the friction and also limit oil consumption.

Andersson [1] showed the distribution of fuel energy usage for a medium sized passenger car and reported that the piston assembly is a major source of losses and responsible for about 40-50% of the total mechanical losses during an urban cycle. Other work [2] showed that the piston ring contribution to the entire friction loss is 19% in a light duty vehicle. Many laboratory tests have been carried out to measure frictional losses between the piston assembly and cylinder liner using the 'floating liner' method [3, 4, 5] or 'indicated mean effective pressure' (IMEP) method [6, 7]. However, there are several drawbacks to these techniques. Intensive modifications and instrumentation of the test engine inevitably increase the time and the cost of laboratory tests. They also do not give a clear picture for the contributions to frictional losses of the individual parts (*i.e.* piston rings or piston skirt). Particularly in a fired engine, there are many factors effecting the lubrication of the piston assembly such as blow-by, dynamics of the piston and ring and thermal deformations.

As an alternative method, simplified test rigs have been developed to investigate the piston ring lubrication mechanism and the related friction phenomena. The designs of these test rigs are wide ranging and depend on the focus of the research. Although whole piston and cylinder liner assemblies have been used in certain designs [8] a typical test rig configuration consists of segments of a piston ring and cylinder liner where one of them reciprocates and the other is kept stationary [9, 10, 11, 12]. These components are tested for different operating parameters, *i.e.* speed, load, viscosity and lubricant rate. Since most of these parameters are controllable, bench tests provide detailed information about how the different parameters influence the piston ring lubrication.

Akalin and Newaz [12] developed a reciprocating test rig to simulate the engine piston ring and liner contact. A ring holder was modified from the ring holder design developed by Hartfield *et al.* [13]. Friction force between the piston ring and liner was measured using strain gauges placed on a cantilever beam connecting the ring holder to a loading arm. They also developed a mixed lubrication model to predict the lubrication and friction characteristic of the piston ring and liner contact. The results highlighted that temperature, surface roughness and running speed were important parameters for identifying the lubrication regime. However, normal load had a slight effect on the friction coefficient under the simulated mixed lubrication condition. In general, the analytical results and the bench test results were well matched. Like Akalin, Bolander *et al.* [11] developed a test rig to correlate with a numerical model of the piston ring-liner interface. However, in their design a three axis force transducer was used to measure the normal, tangential and side loads generated on the piston ring segment. Depending on the test rig operating conditions, the entire range of lubrication regimes, from boundary to full-film hydrodynamic lubrication, were observed at different points in the stroke. As expected the highest friction occured in the mixed and boundary lubrication regimes.

The lubricant film formed between the piston ring and cylinder liner is very thin and the measurement of this essential variable is difficult. In literature, several methods have been applied to measure oil film thickness in piston rings such as capacitance [14, 15, 16], resistance [17] and the laser induced florescence method [18, 19]. All of these methods have some degree of success;

however, these methods require the need to penetrate the cylinder liner in order to access the ring-liner conjunction.

The ultrasound technique is based on sensing the reflections from the ring-liner contact; therefore the ultrasonic sensors do not have to be mounted flush with the inner liner surface. Post grinding of the liner could be enough to place the sensors on the liner. This provides localised non-invasive measurements. Recently, the method was applied to a motored engine to measure the film thickness between the piston ring and cylinder liner [20]. However, there occured a resolution problem due to the sensor size (*i.e.* the ultrasound pulse was emitted over a larger area than the piston ring contact). In this study, smaller piezo-electric sensors were used to enhance the spatial resolution and the piston ring-contact was simulated using a Plint high frequency reciprocator. The average minimum film thickness was measured at five different locations and the ring-liner friction force was measured over the entire cycle. Furthermore, an all-regime numerical model is used to predict the pressure profile, film thickness and friction force. The experimental results were compared to the numerical predictions.

2 Test Apparatus

In this section the test equipment, instrumentation and test specimens will be introduced as well as the perparation of the ultrasound sensors.

2.1 Piston Ring-Liner Simulator

In this work a Plint TE-77 high frequency reciprocating tribometer combined with an ultrasonic pulsing system. The TE77, schematically shown in Fig. 1, is a flexible tribometer that has been used in several other piston ring-liner wear studies [13, 21]. The machine configuration involves a special adapter oscillated mechanically over a fixed liner section. The adapter retaining a section of piston ring is loaded against the liner section by a spring balance through a lever and stirrup mechanism. The normal force is transmitted directly onto the moving specimen by means of a needle roller cam follower on the adapter and the running plate on the loading stirrup. The oscillations are produced by a variable speed motor with an eccentric cam, scotch yoke and guide block arrangement. A stable oscillating frequency is maintained by a tacho generator feedback system. The whole assembly is mounted on flexible supports, which allowed free movement in the horizontal reciprocating axis. A stiff piezo-electric force transducer connected to the assembly measures the friction force in the reciprocating direction. Due to the liners horizontal position, it is useful to identify the dead centres where the oscillating ring stops. The dead centre closest to the friction sensor is named top dead centre (TDC) and the one closest to the adapter mounting hole is named bottom dead centre (BDC) in this work.

2.1.1 Test Specimens

In this study, a pair of cast-iron liner and ring segments from a heavy duty diesel engine were used to create the contact. The liner specimen was cut from a production cylinder liner with a bore diameter of 130 mm. The liner specimen, 50 mm in length and 20 mm in width, has a cross-hatched surface finish typical of the honing process, as illustrated in Fig. 2. Both the cylinder liner and piston ring have been run-in in a fired engine prior to these tests. The pro-

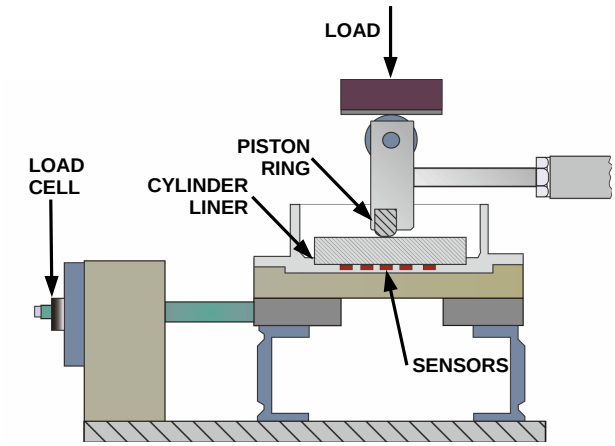

Figure 1: Plint TE-77 simulated piston ring-liner contact schematic.

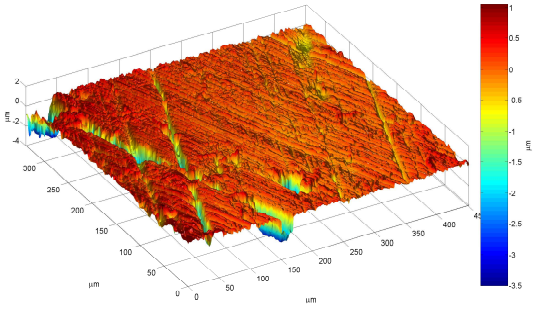

Figure 2: 3D image of cylinder liner surface used in the tests, measured with a Confocal microscope

duction engine piston ring was sectioned into a length of 45 mm and a thickness of 3 mm. The piston ring has an asymmetric barrel shaped face as illustrated in Fig. 3.

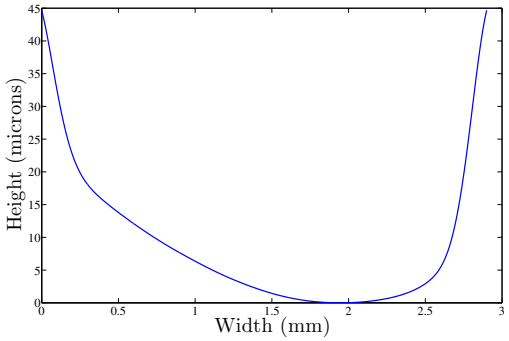

Figure 3: Piston ring profile measured by a profilometer with a Gaussian filter applied

2.1.2 Conformability of the Ring-Liner Contact

Consistent conformability between the piston ring and cylinder liner is necessary from test to test. In the engine, the ring is able to conform due to its inherent tension and freedom to move. However, in simulated test rigs, the uncompressed piston ring (the diameter of the ring is bigger than the diameter of the liner) would mean that in it's free state the piston ring would only make contact at the edge of the liner. To prevent this, a special ring holder manufactured from an original production piston was designed and attached to the adapter (see Fig. 4). The conformability of the ring-liner contact was adjusted by two slotted plates located at either side of the ring holder and a grub screw in the centre which pushed the ring from behind. The liner specimen was held in the lubricant bath and secured by six grub screws allowing for axial and lateral alignment of the liner. Fujifilm Prescale pressure measuring film was used to check the conformability of the contact. The Fujifilm paper indicating the stages of the ring-liner contact from the initial to final set-up are shown in

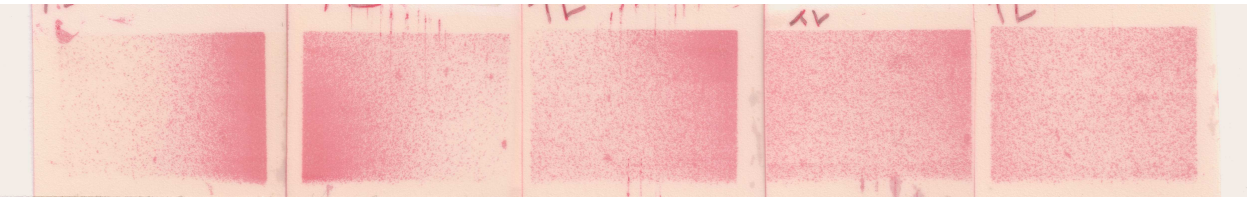

Figure 5: Fujifilm Prescale pressure measuring film used during the conformability adjustment, from the initial attempt (left) through to the conformal contact (right).

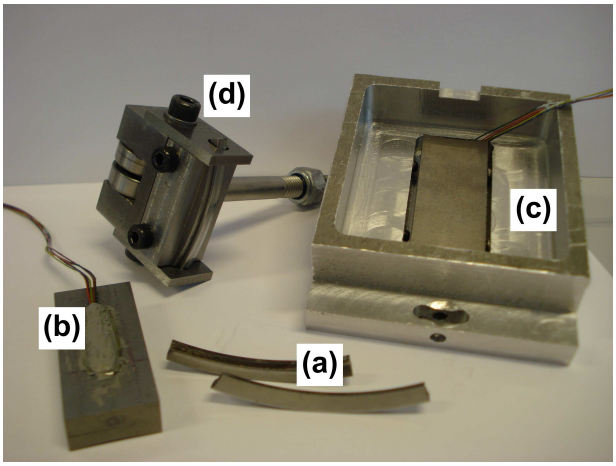

Figure 4: Piston Ring Adapter and Holder, (a) Piston Ring sections, (b) Cylinder liner section with ultrasonic transducers attached to the back side, (c) Oil bath and cylinder liner holder, (d) Ring adapter.

Fig. 5. The progress of obtaining conformability is clear from the initial to final set-up. The ring-liner contact was initially unconformal such that a more dense pink colour appeared at the right hand-side of the liner, indicating a higher contact pressure. After a few adjustments, a more conformal contact where the colour is evenly distributed over the liner surface has been obtained.

2.2 Ultrasonic Sensors

10 MHz piezoelectric crystals with a width of 1.3 mm and a length of 2.5 mm were used to generate ultrasonic waves. The bonding surface should be free from pits and irregularities and the back of the liner sample was therefore ground to provide a flat mounting surface for the piezo-crystal sensors. An epoxy resin formulated specifically for bonding strain gauges was applied and five piezo-crystal sensors were glued on to the back side of the liner by means of a guidance template indicating the sensor positions. The electrodes of the sensor were connect to a small coaxial cable, with a diameter of 0.4mm, and covered by a layer of silicone.

These five ultrasonic sensors placed at the back of the liner were almost equally distributed. The central sensor was positioned at the middle of the stroke by adjusting the liner holder's grub screws located in the axial direction. Thus, the ultrasonic sensors were kept in the stroke area swept by the piston ring and they were able to record the oil film data at five locations between the dead centres. The sensor positions over the liner are given in Table 1 where the measurements are taken relative to TDC.

Table 1: Sensor's location over the stroke

		Distance from TDC (mm)
TDC		0
Sensor Number	1	1.42
	2	4.08
	3	7.27
	4	10.40
	5	13.28
BDC		15.00

Table 2: Properties of the lubricant used in the tests.

Density, ρ	843.4 kg/m^3
Kinematic Viscosity at 40°C, μ	37 cSt
Kinematic Viscosity at 100°C, μ	6.5 cSt
Longitudinal wave velocity, c	1440 m/s

2.3 Instrumentation

An ultrasonic pulsing unit embedded into a dedicated computer was used. This unit consists of an ultrasonic pulsing and receiving card (UPR) which is equipped with 8 channels and a maximum achievable pulse rate of 80 kHz on a solitary channel. Receiver gain range is between -40 db and +110 db and the receiver bandwidth is from 0.1 to 25 MHz. Each of the ultrasonic sensors was individually connected to the pulsing unit, totalling 5 channels with a pulse repetition rate of 15 kHz for each. The sensors were excited by short duration high voltage signals and thus ultrasonic pulses were generated. These pulses propagated through the liner specimen. The system operated in a pulse-echo mode, meaning that the reflected pulses from the ring-liner conjunction were also received by the sensors. Ultrasonic reflection signals were digitised at 100 MHz with a 12 bit resolution. The digitised data was recorded to hard disk in binary file format and then a post-processing software program translated the data to oil film thickness. The piezo-electric transducer (Kistler type 9203) with a range of ±500 N and normal sensitivity of 50 pC/N was used to measure the friction force. The charge amplifier (Kistler type 5007) converts the charge produced by the transducer into proportional electrical signals with a resolution of 0.001 N. The transducer was calibrated with a known load before the experimental stage. Friction data output was logged to the computer hosting the ultrasonic pulsing unit.

2.4 Lubricant

The lubricant used in this study was a pure base oil. The physical properties of the lubricant are given in Table 2. The liner specimen was fully immersed in a pure base oil without an additive package. This does not represent the real lubricant condition in the engine, which would normally be significantly less. However, it ensures that the inlet is fully flooded allowing for good, accurate comparisons with the numerical model. It also assists in maintaining a stable temperature of the liner surface during the short tests. The oil bath temperature was logged at a stable 22°C throughout the tests. The ASTM D31 equation was used to calculate the lubricant viscosity at 22°C;

$$log(log(\mu + 0.7)) = A - B \cdot log(T + 273.15), \quad (1)$$

where ν is viscosity, A and B are constants and T is temperature. Using the values in Table 2,

$A = 8.8686$ and $B = 3.4743$, giving a viscosity of 85.66 cSt or 0.072 $Pa \cdot s$.

3 Ultrasonic Oil Film Measurement

In this section the method for processing the ultrasound signals will be discussed.

3.1 Background

The proportion of an ultrasonic pulse that is reflected from a perfectly bonded interface is known as the reflection coefficient and varies with the acoustic properties of the matching materials. This proportion is given by Eq. (2), where z_1 and z_2 are the acoustic impedance of the materials either side of the interface.

$$R_{12} = \frac{z_1 - z_2}{z_1 + z_2} \tag{2}$$

However, the ring-oil-liner layer can be modelled as a quasi-static spring. Tattersall [22] demonstrated that the reflection coefficient of a thin layer was given by;

$$R = \frac{(z_1 - z_2) + i\omega/K(z_1 z_2)}{(z_1 + z_2) + i\omega/K(z_1 z_2)} \tag{3}$$

where ω is the angular frequency of the ultrasonic wave ($2\pi f$) and K is the stiffness of the interfacial layer. If the layer consists of a liquid, the stiffness of the layer depends on its bulk modulus and thickness ($K = B/h$). The bulk modulus can be written in terms of the speed of sound, c, and density, ρ, of the layer material ($B = \rho c^2$). This gives,

$$K = \frac{\rho c^2}{h} \tag{4}$$

This stiffness can be used in the quasi-static spring model for identical materials either side of the interface ($z_1 = z_2$) then equation Eq. (3) becomes:

$$h = \frac{\rho c^2}{\pi f z}\sqrt{\frac{|R|^2}{1 - |R|^2}} \tag{5}$$

where $|R|$ is the modulus of the reflection coefficient. This relationship gives the layer thickness in terms of reflection coefficient and acoustic properties of the oil and materials either side of the interface. More detail about ultrasound film thickness measurements can be found in reference [23].

Experimentally, as the sensor is coupled to a test specimen, some of the incident wave is transmitted forward and the remainder is reflected back. The reflection coefficient can be obtained by,

$$R = \frac{A_r}{A_i} \tag{6}$$

where A_i is the incident wave amplitude and A_r is the reflected wave amplitude. However it is difficult to measure the incident pulse. Hence in practice it is convenient to record a reflection from the liner-air interface, called the reference interface, because most of the acoustic energy emitted from the sensor is reflected back due to a high acoustic mismatch between the materials. Therefore the reflected wave is almost equal to the incident wave. Eq. (6) shows that for such an interface, R tends to one. This ultrasonic approach has been used previously to monitor the condition of a lubricant film in machine elements [24, 25, 26].

3.2 Data Analysis

The ultrasonic reflections captured by the sensors were continuously recorded as the test was

in progress. In this section, only the data captured by sensor 1 has been used to explain the data processing technique. The same procedure has also been applied to the other sensors to obtain the oil film thickness. Fig. 6a shows reflections from the liner specimen in the time domain. The first pulse (I) is a combination of reflection from the back side of liner and sensor initiation. The second pulse (II) is reflected from the inner side of liner. This 'II' pulse is isolated from the rest of the signal and successively recorded during the test. Before starting the test, the reference pulse from the liner-air interface was recorded. Fig. 6b shows two reflections, the reference pulse and ring pulse recorded as the ring passes over the sensing area, superimposed on a single graph. The amplitude of the signal decreases because some of the ultrasound energy passes through the oil into ring.

Fig. 6c shows a sample of these successive signals as the piston ring reciprocates over the liner. In the figure, each trough, where the pulses are reflected from the piston ring, corresponds to one of the ring traversals over the sensor area. A fast Fourier Transform (FFT) was performed on the reference pulse and each of these successive reflected pulses. Thus diving all FFT amplitudes of the successive pulses by the amplitude of reference pulse gives the reflection coefficient spectra (*i.e.* R versus f). The centre frequency was used to determine the reflection coefficient. Fig. 6d shows the reflection coefficient against pulse number. In the figure, each trough, where the pulses are reflected from the piston ring, corresponds to one of the ring travels over the sensor area. It is seen that the piston ring has passed over the sensing area six times and there are two repetition intervals between the troughs, short and long, since the sensor 1 is close to the TDC. The lubricant film thickness can be obtained by substituting the reflection coefficient data into the spring model, Eq. (5). Fig. 6e shows the oil film thicknesses which were obtained from the data given in Fig. 6d. One ring passage has been represented by approximately 100 pulses (see Fig. 6f) and this number depends on pulsing rate of the ultrasonic system and the ring reciprocating speed.

4 Numerical Model

A numerical model of the experiment has been developed in order to predict both the film thickness and friction that is also measured experimentally. As it is assumed that the piston ring-cylinder liner contact runs in the mixed lubrication regime for at least some of the stroke, a model must be developed that calculates both the hydrodynamic film pressure and asperity contact pressure.

As the contact profile is converging-diverging, some cavitation will occur along the trailing edge of the ring. In order to solve the Reynolds equation incorporating cavitation, a modified version of the Giacopini *et al.* [27] mass-conserving cavitation algorithm was used. More precisely, a two dimensional time dependent solution of the averaged Reynolds equation was formulated as a Linear Complimentary Problem (LCP) where the film thickness was replaced with flow factors,

$$\begin{aligned} \nabla \cdot (A_0 \nabla p_0) - \lambda \nabla \cdot (B_0) - \gamma \frac{\partial}{\partial t} \left(\bar{h} \right) \\ + \lambda \nabla \cdot (r B_0) + \gamma \frac{\partial}{\partial t} \left(r \bar{h} \right) = 0 \\ p_0 > 0 \\ r > 0 \\ p_0 r = 0 \end{aligned} \tag{7}$$

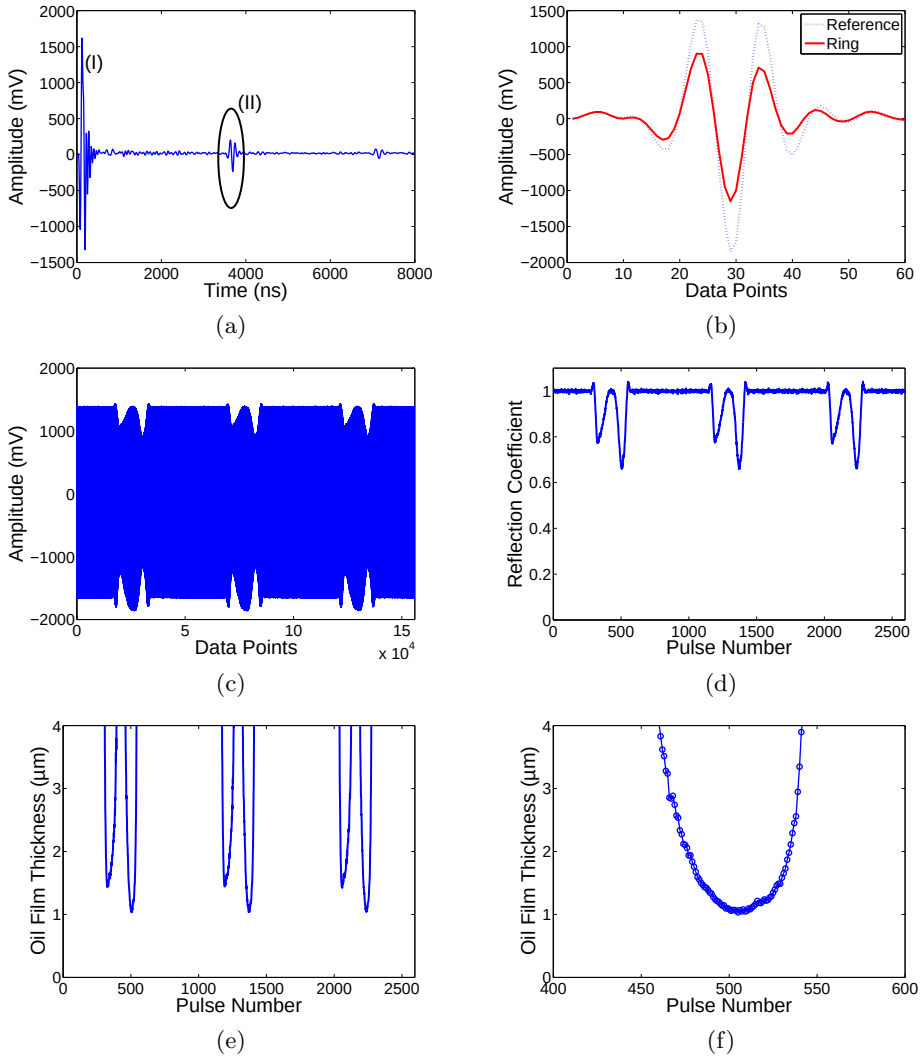

Figure 6: Data analysis graphs for Sensor 1: (a) a typical waveform showing the reflections from liner specimen, (b) extracted pulses from the inner side of the liner, (c) successively recorded pulses as the piston ring reciprocates, (d) reflection coefficient at centre frequency, (e) oil film thickness, (f) close-view of one ring passage over the sensing area.

where A_0 and B_0 are flow factors calculated according to the method found in [28], p_0 is the averaged film pressure, r is the complimentary variable and λ and γ are constants (defined in the nomenclature). $\bar{h}$ is defined as;

$$\bar{h} = h_0(t) + \frac{1}{l_1 l_2} \int h_r(x, y) dy \qquad (8)$$

where h_0 is the separation between the piston ring and cylinder liner, h_r is the liner roughness (see Fig. 2) and l_1 and l_2 are the length and width of the roughness measurement. For the boundary conditions, p_0 and r were defined as zero at the inlet, outlet and sides on the contact.

The LCP problem, Eq. (7), was solved using the finite difference method where the p_0 terms were central differenced and the r terms upwind differenced. The solution domain was divided into 50 by 10 nodes (50 in the entraining direction, 10 across the width) which was found to make the film thickness and friction independent of grid size.

The problem is considered smooth on the solution domain and the surface roughness is incorporated in the flow factors, A_0 and B_0. These are calculated using the technique described in [28] over the liner surface illustrated in Fig. 2. It is assumed that the piston ring is smooth in comparison to the cylinder liner surface. When the surfaces come into contact the deformation is found using a boussinesq-type elasto-plastic contact mechanics model. The whole technique is described in detail by Sahlin *et al.* [29, 30] and will not be repeated here.

The problem was divided into 100 time steps. Increasing the number of time steps did not affect the solution. At each time step the crank angle (θ) was found and then the velocity of the piston ring was calculated from Eq. (9):

$$U = \pi N s \cdot \cos(\theta), \tag{9}$$

where N is the rotational speed of the Plint machine in Hz and s is the stroke. Once the velocity is known a force balance is solved where the film thickness is calculated which balances the applied load with the hydrodynamically supported load and the load supported by asperity contact (from the contact mechanics model [29, 30]). Once this is complete the problem can be incremented one time step and the process repeated. As Eq. (7) is time dependent and therefore depends on the previous time step the solver must be run through approximately 1.1 full cycles for convergence to be reached with the previous cycle. Convergence is assumed when the film thickness and derivative of film thickness is within 1% of the previous cycle.

Friction (f_{tot}) is calculated as the sum of viscous friction f_{hyd} and boundary friction f_{bd}. Boundary friction is calculated as;

$$f_{bd} = \eta \int_{\Omega} P_{CP} dA \tag{10}$$

where η is the dry friction coefficient and P_{CP} is the average asperity contact pressure, found from the contact mechanics model. The dry friction coefficient, taken as 0.192, was found by running a reciprocating test with no lubricant present. Hydrodynamic friction is calculated as;

$$\begin{aligned} F_{hyd} = &- \int_{\Omega} \mu U \left(\frac{\bar{1}}{h} + 6c_{11} \right) \\ &- \left(\left(-\frac{\bar{h}}{2} + d_{11} \right) \frac{\partial p_0}{dx} + d_{12} \frac{\partial p_0}{dy} \right) dx \end{aligned} \tag{11}$$

where $\bar{h}$ is the average separation and c_{11}, d_{11} and d_{12} are flow factors calculated as described in [29, 30].

5 Results and Discussion

In this section the film thickness measured with ultrasound will be presented as well as comparisons of film thickness and friction with the numerical model.

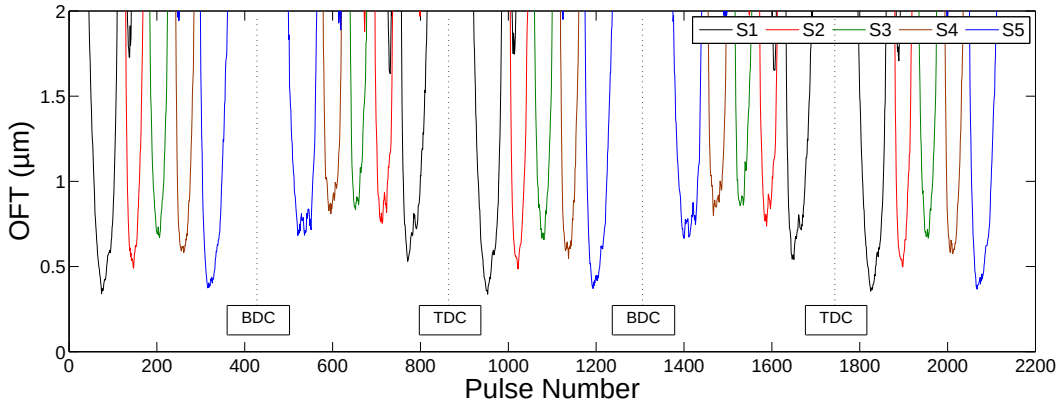

Figure 7: Typical measurement result travels on the liner

5.1 Measured Film Thickness

If an array of the successive pulses of interest (*i.e.* pulse (II) in Fig. 6a) individually captured by the sensors is analyzed, the film thickness values at the fixed sensor locations can be obtained. These film thickness values can be superimposed on a single graph. Fig. 7 shows the measurements of film thickness as the ring reciprocates at 2.5 Hz under a normal load of 80 N. In the figure, the ring starts its travel from TDC to BDC, thus it is initially captured by sensor 1 (*i.e.* close to TDC). As the ring moves from one sensing area to the next, the other sensors detect the ring respectively. This roughly provides an overview of lubricant film formation over the stroke. It is notable that the film thickness data from cycle to cycle was very repeatable. The horizontal axis in the figure is given in terms of pulse number, however this could be converted to time if the pulse rate (indicating how many ultrasound pulses are sent through the liner specimen in a second) is known. In this case the pulse rate is 2000 pulses per second. This was also confirmed because it can be seen in the figure that two and half cycles were observed in one second at 2.5 Hz (2.5 rev/sec).

During testing, there were some blurring effects on the measurements, especially in the case of the ring travelling from BDC to TDC. This is because the interface between the ring and liner is not homogenously filled with lubricant due to cavitation occuring. If the oil is partly depleted under the sensing area, this leads to more ultrasound reflected from the interface due to an air-oil mixture in the contact (*i.e.* resulting in bigger reflection coefficients) and the impression of greater film thickness measurements being recorded. The ring profile is not symmetric, but has a different diverging shape in each direction which influences the lubricant condition in the contact and how much cavitation occurs. The ring was installed in the ring holder with the greater converging shape facing towards BDC. Because of this profile, normally a higher film thickness would be expected on the down stroke from TDC to BDC. However, because there is a far larger cavitating region on the up stroke, from BDC to TDC, the ultrasound recorded an anomalously high film thickness in this direction.

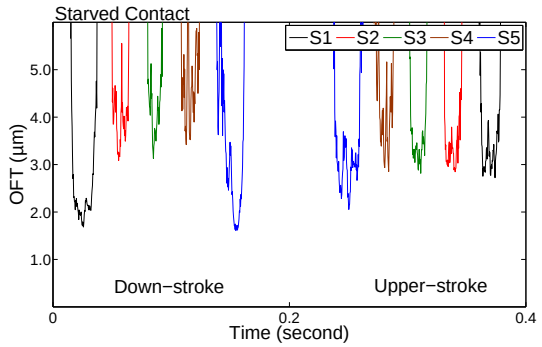

(a)

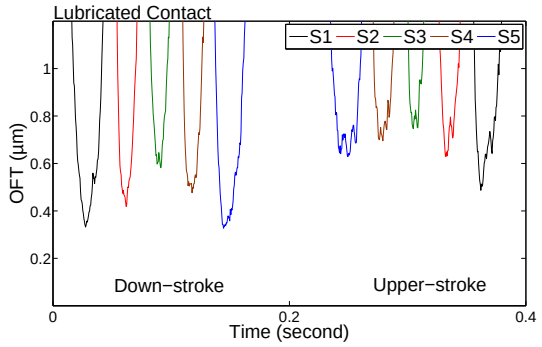

(b)

Figure 8: Measured film thicknesses for one complete cycle: (a) starved and (b) flooded contact conditions under 60 N at 2.5 Hz.

A test was carried out by providing a smaller amount of oil into the contact to show the effect of oil availability on the measurement. The results taken from starved and flooded conditions are both given in Fig. 8a and Fig. 8b.

Under the same loading and reciprocating speed, the blurring of the ultrasonically measured ring profiles was more visible for the starved condition. Additionally, cavitation which occurs in the diverging part of the contact is responsible for this blurring of the profile. The non-symmetric barrel shaped piston ring leads to a different size of the cavitation region according

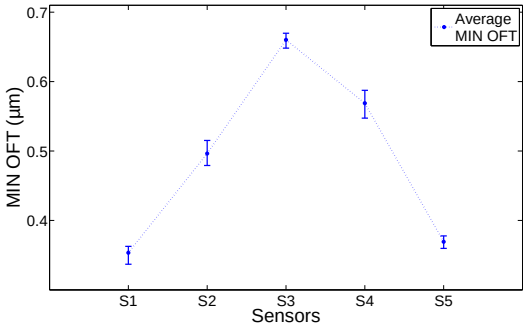

Figure 9: Minimum film thickness for down stroke (Normal load: 80N, reciprocating speed: 2.5 Hz)

to the direction of the stroke [31]. The cavitation region on the down stroke is considerably less than that on the up stroke because the diverging part of the ring is much smaller in down stroke than in the up stroke. This can be seen in Fig. 8b where the small blurring for the up stroke was also observed in the fully flooded contact test. The inhomogeneous film layer (air-oil mixture) was the main source of the noise in the signal, leading to thicker films being recorded during the up stroke. In this study, the down stroke data exhibits far less blurring (noise) and been used for comparison with the numerical model. It was concluded that the up stroke data cannot be considered reliable due to excessive cavitation. An example of the minimum oil film thicknesses (MOFT) measured by the sensors is given in Fig. 9 where the MOFT data represents the mean value of a series of cycles and the standard deviation gives an indication of cycle to cycle variation. As illustrated in the figure, towards sensor 3 where lubricant entrainment speed is highest, the oil film thickness becomes largest due to the hydrodynamic lift of the piston ring.

5.2 Comparisons between Experimental and Numerical results

In the following section the results from the numerical model will be compared with the values measured experimentally, firstly in terms of friction and then oil film thickness.

5.2.1 Friction

In this section the total friction calculated from the simulations, a combination of both boundary and hydrodynamic friction, is compared with the friction force measured from the force transducer in the experiment. Fig. 11 gives a comparison of the experimental and simulated friction for two different operating conditions, both with the same speed of 15Hz but with a low load of 40N and a high load of 100N. Fig. 12 again compares experiment and simulation, but this time with a constant load of 60N and a low speed of 10 Hz and a high speed of 17.5 Hz. Analysing the results, it is noticeable that there is a large difference in film thickness around TDC, or 0° crank angle. In the simulation, boundary lubrication is predominant until approximately 35° crank angle when the sliding speed becomes sufficiently high to allow for the surfaces to become fully separated by the hydrodynamic affect. At this point the boundary friction contribution dramatically reduces and only the viscous friction component is left, giving the sudden drop in friction force. However, in the experiment the friction force drops far more quickly at approximately 15° crank angle. It is proposed that this is due to the dynamics of the test rig, leading to stick-slip occurring. When the sliding speed approaches zero at TDC, the ring comes into asperity contact with the liner and friction increases dramatically. As the ring sliding speed increases again, the ring 'sticks' and then suddenly 'slips' due to the difference in static and dynamic coefficients of friction. This can be evidenced by the 'rippling' that occurs as the friction suddenly drops.

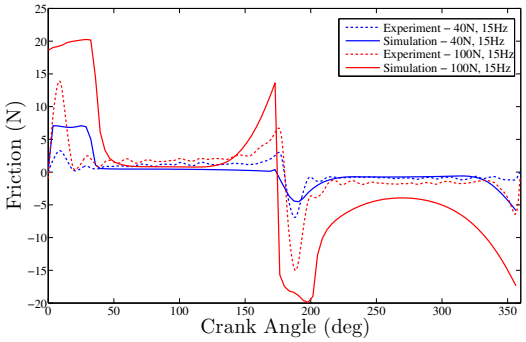

Figure 10: Comparison of experimental and simulated friction for a constant speed of 15Hz and loads of 40N and 100N.

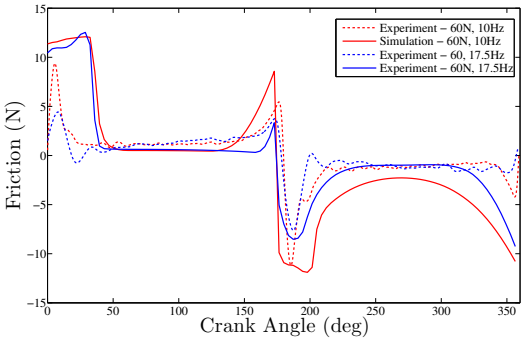

Figure 11: Comparison of calculated and measured friction for a constant load of 60N and speeds of 10 Hz and 17.5 Hz.

During the midstroke the lubrication is predominantly hydrodynamic and there is a much closer match between simulation and experiment. Any difference here is most likely caused by an inaccurate value of lubricant viscosity be-

ing used in the simulation, as this is an estimate at 22° C based on the provided lubricant data.

At BDC, or 180°, as the friction increases again there is less difference between experiment and simulation as was present at TDC, with the values matching well. This is probably because, due to the asymmetric ring profile, there is a larger film present on the downstroke and so at BDC the film thickness is greater (due to the squeeze effect) and so the issues encountered at TDC with the very low film thickness are less prevelant.

5.2.2 Film thickness

In this section the minimum oil film thickness calculated with simulation, and measured at the five sensor locations, is compared. Fig. 12 illustrates this data at a constant speed of 10Hz with a low, medium and high load. From Fig. 12 it

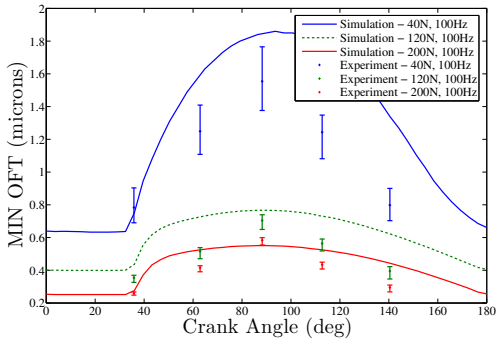

Figure 12: Comparison of calculated and measured film thickness at a constant speed of 10Hz and loads of 40N, 120N and 200N.

can be seen that the experimental data correlates reasonably well with simulation. In general, the simulation overestimates the minimum oil film thickness when compared to the experiment. It is suggested that the predominant reason for this is due to the value of viscosity used in the simulation, as was mentioned previously when discussing the friction results. It is unknown exactly what the effective viscosity was in the contact. For example, it is inevitable that some shear heating of the lubricant will take place during sliding and this increase in temperature will reduce the viscosity of the lubricant. A lower viscosity would cause lower film thicknesses, as shown experimentally.

Another source of error is the assumption of contact geometry. Although this was measured accurately (see Fig. 3) and the ring adapter was aligned to make sure it sat flat and parallel with the liner sample, it is possible that there could be some small misalignment leading to a slightly different ring profile, giving different converging and diverging shapes and therefore a slightly different film thickness.

Also, it must be remembered that the ultrasound technique must assume a density and speed of sound in the lubricant in the contact, which are assumptions from the bulk properties and may introduce some errors in the calculation of film thickness.

6 Conclusion

Reciprocating tests have been performed between a section of piston ring and cylinder liner with the following conclusions;

1. Ultrasound proves an effective way of measuring film thickness, an invaluable aid for understanding the lubrication regime in a tribological contact and for validating simulations.

2. Cavitation occurs in the contact which can adversly effect the ultrasonic measurement

of film thickness, however this is detectable in the reflection coefficient profile and only affected the tests in one sliding direction.

3. The numerical simulation matched well with the experimental data, however the result is sensitive to the value of viscosity used and this is somewhat unknown in the contact.

7 Acknowledgements

Scania AB is thanked for providing components, technical data and discussions. The authors from the Leonardo Centre would like to acknowledge the EPSRC Encyclopaedic Program Grant for funding this work. Support of all the program industrial partners is acknowledged. The authors from LTU would like to thank Stiftelsen för Strategisk Forskning (SSF) and ProViking for also funding this work and the Swedish Research School in Tribology for funding Andrew Spencer's placement at Sheffield University.

References

[1] B.S. Andersson. Company perspectives in vehicle tribology - Volvo. *17th Leeds-Lyon Symposium on Tribology - Vehicle Tribology, Tribology Ser., Elsevier.*, 18:503–506, 1991.

[2] J. A. Spearot. Friction, wear, health, and environmental impacts - tribology in the new millennium. *A keynote lecture at the STLE Annual Meeting, Nashville, Tennessee, May 2000*, 2000.

[3] S. Furuhama and M. Takiguchi. Measurement of piston frictional force in actual operating diesel engine. *SAE Technical Paper Series*, 790855, 1979.

[4] S. Furuhama and S. Sasaki. New device for the measurement of piston frictional forces in small engines. *SAE Technical Paper Series*, 831284:39–50, 1983.

[5] Y. Wakuri, T. Hamatake, M. Soejima, and T. Kitahara. Piston ring friction in internal combustion engines. *Tribology International*, 25:299–308, 1992.

[6] H.M. Uras and D.J. Patterson. Measurement of piston and ring assembly friction instantaneous imep method. *SAE Technical Paper Series*, 830416, 1983.

[7] R.A. Mufti and M. Priest. Experimental evaluation of piston-assembly friction under motored and fired conditions in a gasoline engine. *ASME: Journal of Tribology*, 127:826–836, 2005.

[8] Y.C. Tan and Z.M. Ripin. Frictional behavior of piston rings of small utility two-stroke engine under secondary motion of piston. *Tribology International*, 44:592–602, 2011.

[9] C. Arcoumanis, M. Duszynski, H. Flora, and P. Ostovar. Development of a piston-ring lubrication test-rig and investigation of boundary conditions for modelling lubricant film properties. *SAE Technical Paper Series*, 952468, 1995.

[10] L.L. Ting. Development of a reciprocating test rig for tribological studies of piston engine moving components - part i: Rig design and piston ring friction coefficients measuring method. *SAE Technical Paper Series*, 930685, 1993.

[11] N.W. Bolander, B.D. Steenwyk, F. Sadeghi, and G.R. Gerber. Lubrication regime transitions at the piston ring-cylinder liner interface. *Proc. IMechE Part J: Engineering Tribology*, 219:19–31, 2005.

[12] O. Akalin and G.M. Newaz. Piston ring-cylinder bore friction modeling in mixed lubrication regime: Part iicorrelation with bench test data. *ASME: Journal of Tribology*, 123:219–223, 2001.

[13] S.E. Hartfield-Wunsch, S.C. Tung, and C.J. Rivald. Development of a bench test for the evaluation of engine cylinder components and correlation with engine test results. *SAE Technical Paper Series*, 932693, 1993.

[14] S.J. Söchting and I. Sherrington. The effect of load and viscosity on the minimum operating oil film thickness of piston-rings in internal combustion engines. *Proceedings of the Institution of Mechanical Engineers, Part J: Journal of Engineering Tribology*, 223:383–391, 2009.

[15] D.O. Ducu, R.J. Donahue, and J.B. Ghandhi. Design of capacitance probes for oil film thickness measurements between the piston ring and linear in internal combustion engines. *Journal of Engineering for Gas Turbines and Power*, 123:633–643, 2001.

[16] A. Dhar, A.K. Agarwal, and V. Saxena. Measurement of dynamic lubricating oil film thickness between piston ring and liner in a motored engine. *Sensors and Actuators, A: Physical*, 149:7–15, 2009.

[17] J.S. Courtney-Pratt and G.K. Tudor. An analysis of the lubrication between the piston rings and cylinder wall of a running engine. *Proceedings of the IMechE.*, 155:155–293, 1946.

[18] T. Seki, K. Nakayama, T. Yamada, A. Yoshida, and T. Takiguchi. A study on variation in oil film thickness of a piston ring package: variation of oil film thickness in piston sliding direction. *JSAE Review*, 21:315–320, 2000.

[19] M. Takiguchi, K. Nakayama, S. Furuhama, and H. Yoshida. Variation of piston ring oil film thickness in an internal combustion engine - comparison between thrust and anti-thrust sides. *SAE paper No. 980563*, 980563, 1998.

[20] E.Y. Avan, R.S. Mills, and R.S. Dwyer-Joyce. Ultrasonic imaging of the piston ring oil film during operation in a motored engine - towards oil film thickness measurement. *SAE International Journal of Fuels and Lubricants*, 3(2):786–793, 2010.

[21] J.J. Truhan, J. Qu, and P.J. Blau. A rig test to measure friction and wear of heavy duty diesel engine piston rings and cylinder liners using realistic lubricants. *Tribology International*, 38:211–218, 2005.

[22] H. G. Tattersall. The ultrasonic pulse-echo technique as applied to adhesion testing. *Applied Physics*, 6:819–832, 1973.

[23] R.S. Dwyer-Joyce, B.W. Drinkwater, and C.J. Donohoe. The measurement of lubricant-film thickness using ultrasound. *Proceedings of the Royal Society A: Mathe-*

matical, Physical and Engineering Sciences, 459:957–958, 2003.

[24] T. Reddyhoff, R. Dwyer-Joyce, and P. Harper. Ultrasonic measurement of film thickness in mechanical seals. *Sealing Technology*, 7:7–11, 2006.

[25] R. Dwyer-Joyce, P. Harper, and B. Drinkwater. Oil film measurement in polytetrafluoroethylene-faced thrust pad bearings for hydrogenerator applications. *Proc. IMechE Part A: Journal of Power and Energy*, 220:619–628, 2006.

[26] M. K. Wan Ibrahm, D. Gasni, and R. Dwyer-Joyce. Profiling a ball bearing oil film with ultrasonic reflection. *Tribology Transactions*, 55:409–421, 2012.

[27] M. Giacopini, M. T. Fowell, D. Dini, and A. Strozzi. A mass-conserving complementarity formulation to study lubricant films in the presence of cavitation. *ASME: Journal of Tribology*, 132:1–12, 2010.

[28] A. Almqvist, J. Fabricius, A. Spencer, and P. Wall. Similarities and differences between the flow factor method by Patir and Cheng and homogenization. *Journal of Tribology*, 133:1–5, 2011.

[29] F. Sahlin, Larsson. R., A. Almqvist, P.M. Lugt, and P. Marklund. A mixed lubrication model incorporating measured surface topography Part 1: theory of flow factors. *Proc. IMechE Part J: Journal of Engineering Tribology*, 224:335–351, 2010.

[30] F. Sahlin, R. Larsson, P. Marklund, A. Almqvist, and P.M. Lugt. A mixed lubrication model incorporating measured surface topography Part 2: roughness treatment, model validation, and simulation. *Proc. IMechE Part J: Journal of Engineering Tribology*, 224:353–365, 2010.

[31] P. Dellis and C. Arcoumanis. Cavitation development in the lubricant film of a reciprocating piston-ring assembly. *Proc. IMechE Part J: J. Engineering Tribology*, 218:157–171, 2004.